Effects of Nickel on Microstructure and Properties of Direct Laser Deposited 00Cr25-XNiMo4 Duplex Stainless Steel

Jing Liang, Lizhao Wang, Yunfei Gao, Suiyuan Chen, Changsheng Liu, Chuang Li, Shixing Yan, and Shiyun Dong

Abstract In this study, the 00Cr25-xNiMo4 Duplex Stainless Steel (DSS) was fabricated by Direct Laser Deposition (DLD) using a YSL-1000 W fiber laser, and the influence of different nickel contents (x = 7.0, 8.0, 9.0, and 10.0 wt%) on the microstructure and properties of the DLDed 00Cr25-xNiMo4 samples were studied. Optimized laser processing parameters were obtained with the laser power 650 W, scanning velocity 6 mm/s. The microstructure of the samples was composed of ferrite and austenite. The percentage of austenite phases in the DLDed 00Cr25Ni9Mo4 DSS samples reached the highest value of 41.8%, which led to the highest tensile strength of 1084 MPa. The yield strength and microhardness of them were 720 MPa and 294.9 $HV_{0.2}$ respectively. The self-corrosion potential of the DLDed 00Cr25Ni9Mo4 DSS samples was −0.228 V, and the self-corrosion current density was 6.410×10^{-7} A/cm^2. Excellent mechanical properties and corrosion resistance with a balance of ferrite and austenite phases were obtained in the DLDed 00Cr25Ni9Mo4 DSS.

Keywords Direct laser deposition · 00cr25-xNiMo4 duplex stainless steel · Microstructure · Mechanical properties · Corrosion resistance

J. Liang (✉) · L. Wang · Y. Gao · S. Chen · C. Liu · C. Li
Key Laboratory for Anisotropy and Texture of Materials, Ministry of Education,
Key Laboratory for Additive Manufacturing and Remanufacturing Materials,
School of Materials Science and Engineering, Northeastern University,
Shenyang 110819, Liaoning, China
e-mail: liangj@atm.neu.edu.cn

S. Yan · S. Dong
Academy of Army Armored Forces, Beijing, China

1 Introduction

Duplex Stainless Steel (DSS) consisting of nearly equal amount ferrite and austenite phases was widely used in the application of propellers, ship impellers, and valve bodies, etc. DSS had better plasticity and toughness than ferritic stainless steel did, which strength was as twice as that of the austenitic stainless steel, meanwhile, its corrosion resistance was excellent [1]. The casting was the main fabricating method for DSS components. The mold design and manufacturing of complex DSS components was difficult. Nonuniformity and defects were easy to appear in some thin-wall parts. DLD used laser directly scanning the feeding powder mixtures to fabricate fully dense metal samples layer by layer without shape limits. According to the characteristics of DLD, complex parts could be fabricated by this method more flexibly [2].

Many researchers had studied the microstructure and properties of DLDed stainless steel recently. Juntao Zhang et al. study the tensile strength (632 MPa) and elongation (46.9%) of the DLDed 304L stainless steel samples under the optimized process parameters were significantly higher than that of the casting samples (tensile strength 485 MPa, elongation 35%) [3]. Zhuqing Wang et al. studied that the grain size (21 µm) of DLDed 304L stainless steel samples under the laser power of 2300 W was smaller than that of the samples under the laser power of 4000 W [4]. Michael A. Melia et al. found that chemical segregation was avoided by increasing the cooling rate or reducing the heat input during the process of direct laser deposition [5].

Peng Guo et al. studied the tensile strength and elongation of the DLDed 316L stainless steel samples with an angle (η) of 0° between the tensile direction and deposition plane were higher 130 MPa and 2.5% than that of the samples with $\eta = 90°$ [6]. Aref Yadollahi et al. found that the microstructure of DLDed 316L SS with longer interlayer time intervals was more uniform [7].

At present, most researches on DLDed stainless steel were concentrated on 316L and 304L SS, while only a few studies were on direct laser deposition of duplex stainless steel. C. J. Wang et al. studied the effects of molybdenum on the properties of DLDed 15Cr21Ni7-xMo (Mo contents were 0, 1, 2, 3, 4 wt%, respectively) DSS. The microhardness of the DLDed 15Cr21Ni7Mo3 DSS samples was the highest (350 $HV_{0.2}$), and the self-corrosion potential of the samples was the lowest of −142.26 mV [8]. C. Zhang et al. used laser additive manufacturing technology and N-containing 2205 DSS powder to repair large structural parts of the ships and marine equipment. The yield strength and tensile strength of the repaired samples were higher 210 and 240 MPa than that of the original used EQ56 structural steels respectively [9].

Researches showed that the ratio of ferrite to austenite in the DLDed duplex stainless steel was difficult to balance because of the fast cooling rates during the DLD process. In the paper, more nickel (one of the austenite forming elements) was added in the DLD processing to adjust the ratio of ferrite to austenite phases. The influences of nickel contents on the microstructure and properties of the DLDed

samples were discussed in detail, and the optimized alloy composition was obtained.

2 Experimental Details

Q 235 steel plates were used as the substrate for the DLD. The element powder mixture with the designed composition (according to the SAF 2507 duplex stainless steel as reference) and particle size ranged from 140 to 200 μm was used. The powder mixture was ball milled for 10 h at a speed of 350 r/min to ensure uniform dispersion of each element. The composition of the powder mixture used in the DLD experiment was shown in Table 1.

A YSL-1000 fiber laser was used for the DLD with argon protection during the processing. The laser spot diameter was 1.8 mm and the overlap rate of each path was 50%. The optimized experimental parameters with the laser power of 650 W, the scanning rate of 6 mm/s were used to fabricate DSS specimens. They were etched with 5 g $FeCl_3$ + 50 ml HCI + 100 ml H_2O solution.

The OLYMPUS-GX71 inverted optical microscope (OM), the JM-6510A scanning electron microscope (SEM), and the TECNAIG220 transmission electron microscope (TEM) were used to analyze the microstructure. Phases identification of the deposited layer was carried out using an X-ray diffractometer (X'PertProMPD-PW3040/60) with Cu target K_α radiation (λ = 1.5406 Å) at 40 kV, 200 mA, the scanning speed 3°/min, and the diffraction angle range 20°–120°. The microhardness was measured by Wilson Wolpert 401MVD digital Vickers hardness tester with the interval distance of 0.2 mm, the load of 200 g, and the loading time of 10 s. The AG-X100KN electronic universal testing machine was used for the tensile test with the tensile speed of 0.5 mm/min. The electrochemical workstation was used for the test of corrosion resistance with the test solution of 3.5% NaCl solution. The test parameters involved scanning range −0.2 to 0.4 V, frequency 10^{-2}–10^5 Hz, and the rate 0.5 mV/s.

3 Results and Discussion

Figure 1 showed that DLDed 00Cr25-xNiMo4 DSS was composed of ferrite and austenite. No other phase in the DLDed 00Cr25-xNiMo4 DSS samples was found through XRD analysis because the cooling rate was very fast during the DLD

Table 1 Chemical composition of Cr-Ni duplex stainless steel alloy powder (mass fraction) %

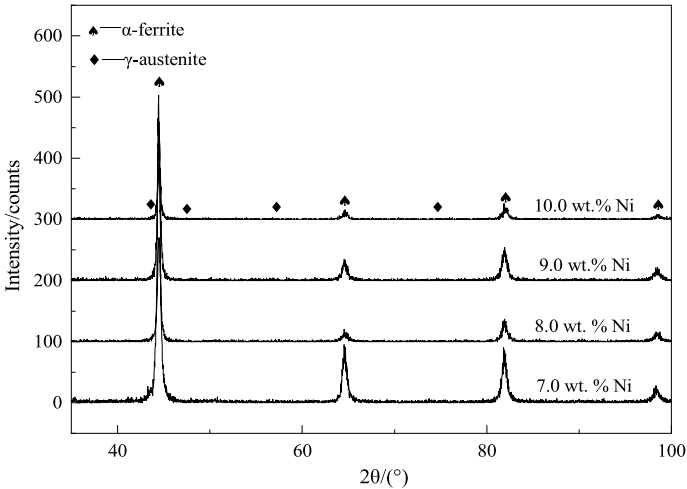| Element	C	Cr	Ni	Mo	Mn	Si	Fe
00Cr25-xNiMo4	0.03	25.00	7.0/8.0/9.0/10.0	4.00	1.20	0.80	Bal.

Fig. 1 XRD patterns of DLDed 00Cr25-xNiMo4 DSS with different nickel additions

process, which was on the left of the TTT curve of the precipitated phases according to the research presented by Feng Shang et al. [10]. With the nickel contents increased, the intensity of ferrite peak ($2\theta = 82.335°$) in XRD patterns overall decreased, which indicated the amount of ferrite decreased while the austenite increased.

Figure 2 showed that with the increase of nickel contents, the percentage of gray phases increased while the white phases decreased. According to the results of XRD analysis, the bright white phases and gray phases were identified as ferrite and austenite respectively. The dendritic austenite was distributed in the ferrite phase boundary. The austenite of Fig. 2c, d were blocky and lamellar respectively.

The amount of ferrite, austenite was roughly analyzed by the grid counting method and the grain sizes of the sample with different amounts of nickel additions were showed in Fig. 3. The amount austenite of the samples reached the highest value of 41.8% when the nickel additions of 9.0 wt%. The grain size of 00Cr25Ni10Mo4 samples (Fig. 2d) was smaller than that of 00Cr25Ni9Mo4 samples (Fig. 2c).

Figure 4 showed SEM images of DLDed 00Cr25-xNiMo4 DSS with different nickel additions. The samples were composed of ferrite (dark gray phases) and austenite (bright white phases). The ferrite was first formed during the solidification of the molten pool. With the temperature decreased, the liquid phase completely transformed into the ferrite and the last austenite precipitated near the ferrite. Under the high cooling rate of the DLD, the nickel additions expanded and stabilized the region of austenite phases. The amounts of nickel at the phase boundary between the ferrite and the austenite were higher than that in the ferrite according to the research presented by V. J. Gadgil et al. [11]. Nickel element diffused from high concentration to lower one which was the driving force for interface movement,
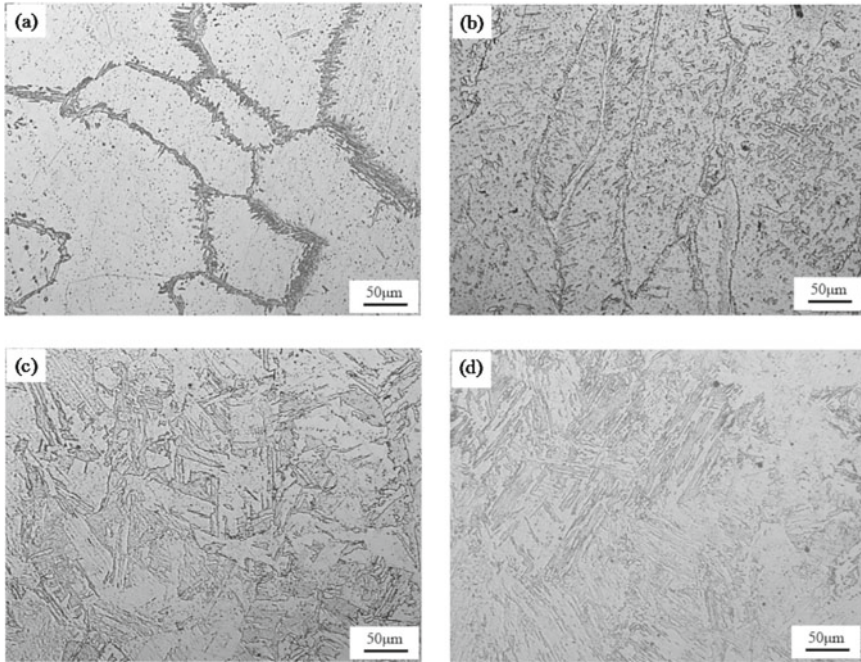
Fig. 2 The morphologies of DLDed 00Cr25-xNiMo4 DSS with different nickel additions: **a** 00Cr25Ni7Mo4 **b** 00Cr25Ni8Mo4 **c** 00Cr25Ni9Mo4 **d** 00Cr25Ni10Mo4
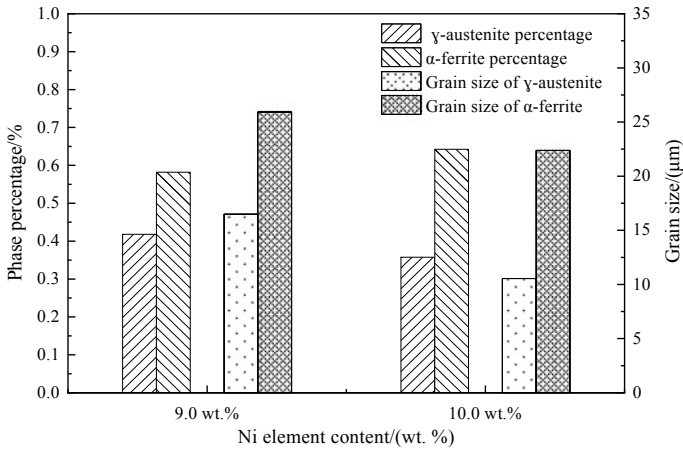

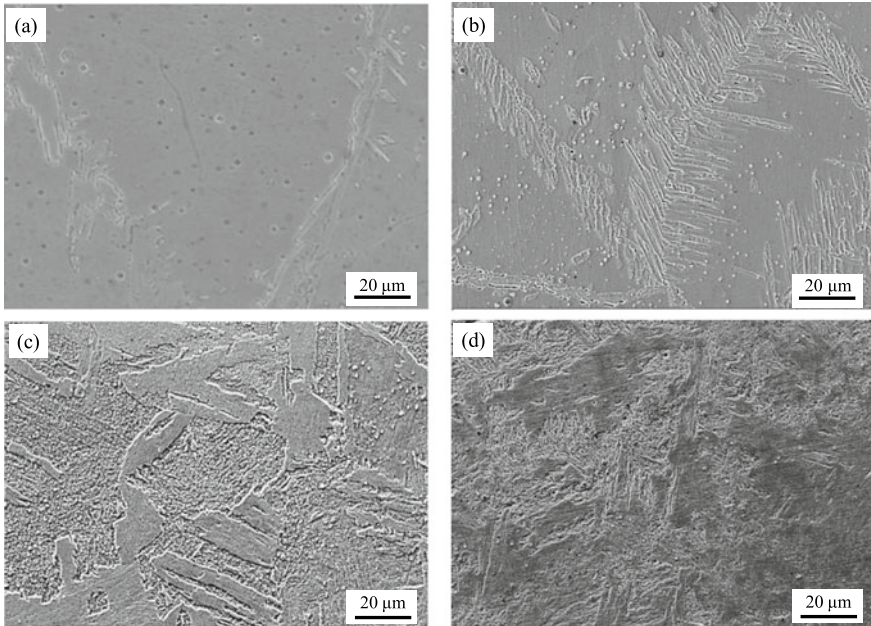**Fig. 3** Phase percentage and grain sizes of DLDed 00Cr25-xNiMo4 DSS with the nickel additions of 9.0 and 10.0 wt%

Fig. 4 SEM images of DLDed 00Cr25-xNiMo4 DSS with different nickel additions: **a** 00Cr25Ni7Mo4 **b** 00Cr25Ni8Mo4 **c** 00Cr25Ni9Mo4 **d** 00Cr25Ni10Mo4

so the austenite grew into the ferrite. Increasing the nickel contents in the samples increased the amount of the austenite phases of the DLDed 25Cr-xNi4Mo DSS samples.

It showed in Fig. 5a, a lot of dislocations were found in the DLDed 00Cr25Ni10Mo4 DSS samples. As reported, the dislocations were caused by the fast cooling rate in the direct laser deposition processing. Figure 5b showed the standard electron diffraction patterns of zone axis [011] of ferrite (body-centered cubic), so A region (black lamellar structure) was lamellar ferrite.
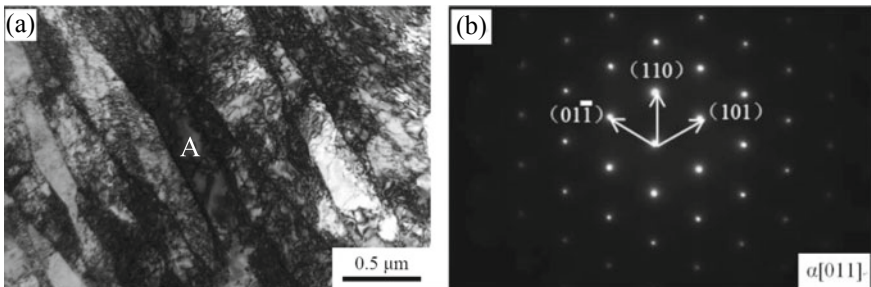

Fig. 5 TEM morphology and electron diffraction pattern of DLDed 00Cr25Ni10Mo4 duplex stainless steel
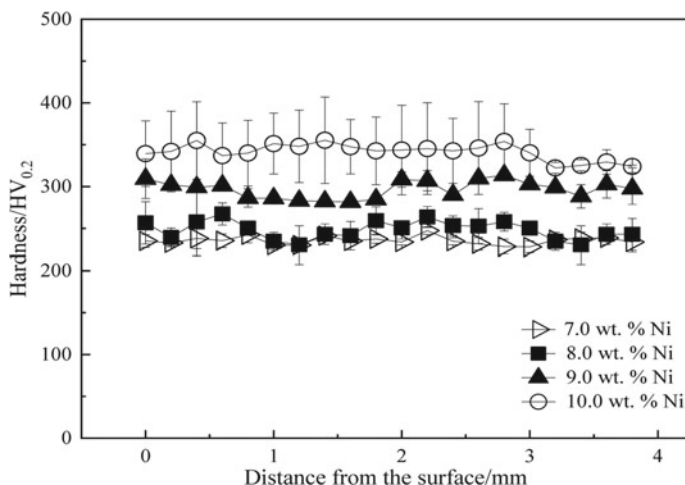
Fig. 6 Variation in Vickers hardness values of DLDed 00Cr25-xNiMo4 DSS with nickel additions of 7.0, 8.0, 9.0, and 10.0 wt%

Figure 6 showed the microhardness distribution of the cross-section to the laser scanning direction of the DLDed samples. With the distance from the deposited layer to the substrate changed, the microhardness of the samples also changed because the DLD process produced the tempering effects on the previous layer when the latter layer was fabricated. The uneven heat diffusion of each layer led to uneven stress distribution. The average microhardness of the DLDed 00Cr25Ni9Mo4 samples was 294.9 $HV_{0.2}$.

Stress-strain curves of the DLDed samples with different nickel contents were showed in Fig. 7. The increase of nickel contents improved the yield strength of the samples because more nickel dissolved in the austenite to form the solution strengthening. Due to the different atomic radius of nickel and iron, nickel replaced the iron in the crystal lattice and caused the lattice distortion. The lattice distortion stress field interacted with the dislocations, hindered the movement of the dislocations, and improved the strength of the samples. The austenite was hard phases, which benefited for the high tensile strength and yield strength. The tensile strength 1084 MPa and the yield strength 720 MPa of the DLDed 00Cr25Ni9Mo4 samples (Fig. 8) with the highest austenite percentage (41.8%) were higher than that of casting DSS.

Potential polarization curves of DLDed 00Cr25-xNiMo4 DSS with different nickel additions were showed in Fig. 9. The samples with nickel contents of 8.0, 9.0, and 10.0 wt% had obvious passivation areas, and the dense passive films were formed on the surface of the samples in the corrosive liquid of 3% NaCl solution. Nickel improved the corrosion resistance of DSS because nickel formed a denser oxide layer than that formed by iron in corrosive solution according to the research
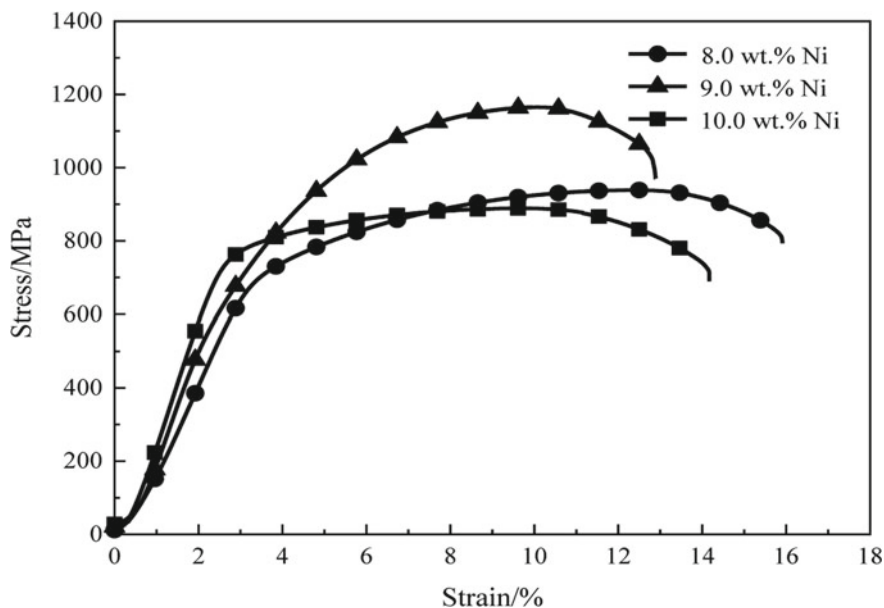
Fig. 7 Tensile stress-strain curves of DLDed 00Cr25-xNiMo4 DSS with nickel additions of 8.0, 9.0, and 10.0 wt%
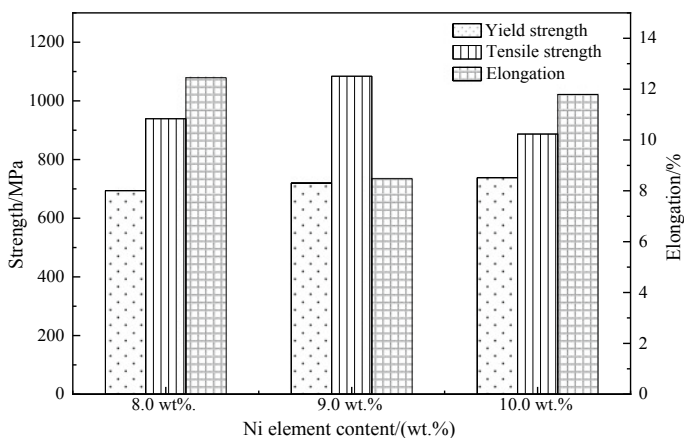

Fig. 8 Tensile properties of DLDed 00Cr25-xNiMo4 DSS with nickel additions of 8.0, 9.0, and 10.0 wt%

presented by X. H. Ma et al. [12]. Figure 10 showed the DLDed 00Cr25Ni9Mo4 samples had the highest self-corrosion potential (−0.228 V) and the lowest self-corrosion current density (6.41 × 10^{-7} A/cm^2).
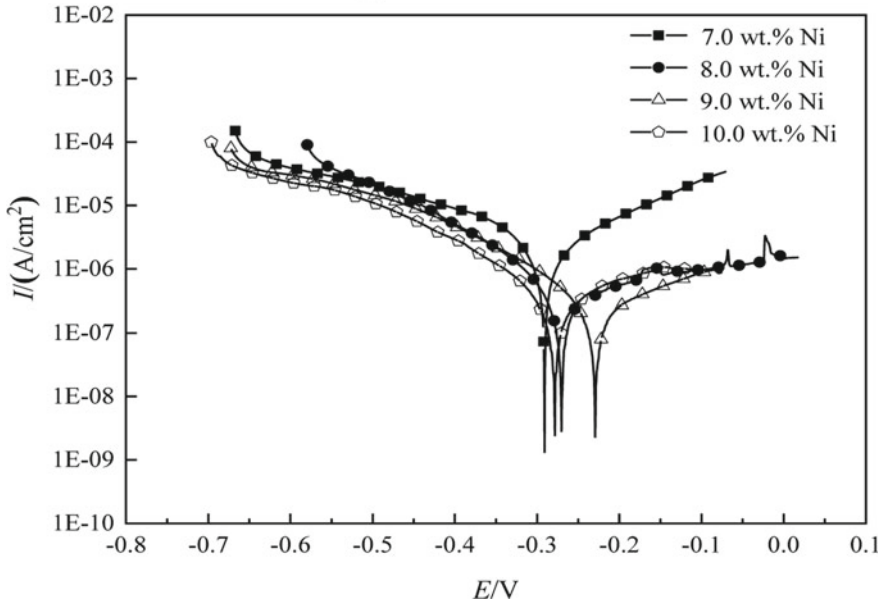
Fig. 9 Tafel curves of DLDed 00Cr25-xNiMo4 DSS with different nickel additions of 7.0, 8.0, 9.0, and 10.0 wt%
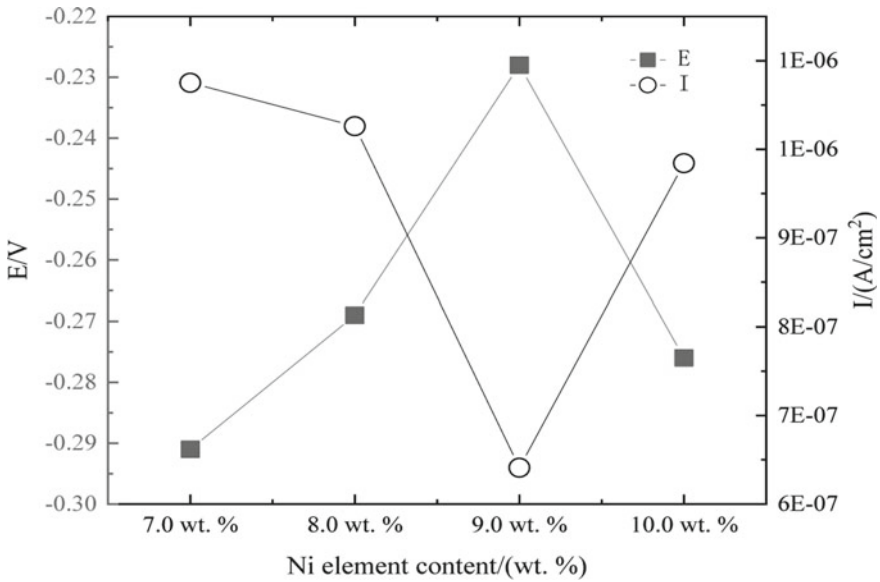

Fig. 10 The self-corrosion potential and the self-corrosion current density of DLDed 00Cr25-xNiMo4 DSS with different nickel additions of 7.0, 8.0, 9.0, and 10.0 wt%

With the increasing of nickel compositions, the corrosion resistance of samples first increased and then decreased. The additions of nickel increased the percentage of austenite and overall refined the grain sizes of ferrite. Nickel was beneficial to the formation of austenite, and the austenite with the face-centered cubic lattice accommodated more alloying elements, thus nickel additions increased the electrode potential of austenite. When the nickel contents of the samples were 9.0 wt%, the balance of austenite and ferrite phases was obtained, and the corrosion resistance of the samples was the highest.

4 Conclusions

The DLDed 00Cr25-xNiMo4 (x = 7.0, 8.0, 9.0, and 10.0 wt%) DSS samples were obtained under optimization processing parameters with laser power of 600 W and laser scanning speed of 6 mm/s.

The DLDed 00Cr25Ni9Mo4 DSS was composed of austenite (percentage of 41.8%) and ferrite (percentage of 58.2%). It had good mechanical properties with the tensile strength of 1084 MPa, yield strength of 720 MPa, elongation of 8.48%, and microhardness of 294 $HV_{0.2}$. The corrosion resistance of DLDed 00Cr25Ni9Mo4 DSS was the best among these 00Cr25-xNiMo4 (x = 7.0, 8.0, 9.0, and 10 wt%) samples with the self-corrosion potential −0.228 V and the self-corrosion current density 6.410×10^{-7} A/cm^2.

References

1. Huang, H., Xu, L., Jing, H., Lv, X.: Droplet transfer characteristics of SAF 2507 super duplex stainless steel CMT + P. Trans. China Weld. Inst. **40**(10), 127–136 (2019)
2. Cheng, Y., Zhao, L., Zhou, K.: Precision casting of 2205 duplex stainless steel inducer. Foundry Equip. Techol. **4**, 20–22 (2018)
3. Zhang, J., Zhang, W., Li, Y., Songhao, H., Huang, S., He, T., Liu, Y.: Laser deposition additive/subtractive hybrid manufacturing process for stainless steel powder based on DMG MORI LASERTEC 65 3D. Mater. Sci. Eng. Powder Metall. **23**(4), 368–374 (2018)
4. Wang, Z., Palmer, T.A., Beese, A.M.: Effect of processing parameters on microstructure and tensile properties of austenitic stainless steel 304L made by directed energy deposition additive manufacturing. Acta Mater. **110**, 226–235 (2016)
5. Melia, M.A., Nguyen, H.-D.A., Rodelas, J.M., Schindelholz, E.J.: Corrosion properties of 304L stainless steel made by directed energy deposition additive manufacturing. Corros. Sci. **152**, 20–30 (2019)

6. Guo, P., Zou, B., Huang, C., Gao, H.: Study on microstructure, mechanical properties and machinability of efficiently additive manufactured AISI 316L stainless steel by high-power direct laser deposition. J. Mater. Process. Technol. **240**, 12–22 (2017)
7. Yadollahi, A., Shamsaei, N., Thompson, S.M., Seely, D.W.: Effects of process time interval and heat treatment on the mechanical and microstructural properties of direct laser deposited 316L stainless steel. Mater. Sci. Eng., A **644**, 171–183 (2015)
8. Wang, C., Liang, J., Chen, S., Liu, C., Shang, S., Chen, Y.: Study on microstructures and properties of direct laser deposited 15Cr21Ni7-xMo stainless steels. Appl. Laser **37**(1), 11–16 (2017)
9. Zhang, C., Zhang, Z., Li, S., Qiu, C., Zhu, S.: Mechanical and corrosion properties of Nitrogen Bearing Duplex stainless steel Sample prepared by laser forming. China Surf. Eng. **32**(2), 163–169 (2019)
10. Shang, F., Chen, X., Wang, Z., Ji, Z., Ming, F., Ren, S., Xuanhui, Q.: The microstructure, mechanical properties, and corrosion resistance of UNS S32707 hyper-duplex stainless steel processed by selective laser melting. Metals **9**(9), 1012 (2019)
11. Gadgil, V.J., Sasse, A.G.B.M., Swens, J.J., Kolster, B.H.: Effect of cooling rate on the austenite-ferrite phase boundary composition of a duplex stainless steel. J. Mater. Eng. **13**, 291–297 (1991)
12. Ma, X.H., Zhang, L., Yang, X.H., Li, Q., Huang, Y.D.: Effect of Ni addition on corrosion resistance of FePC bulk glassy alloy. Corros. Eng. Sci. Technol. **50**(6), 433–437 (2015)